Article

pubs.acs.org/Biomac

Investigations of the Supramolecular Structure of Individual Diphenylalanine Nano- and Microtubes by Polarized Raman Microspectroscopy

Banyat Lekprasert,[†] Vladimir Korolkov,[‡] Alexandra Falamas,[§] Vasile Chis,[§] Clive J. Roberts,[‡] Saul J. B. Tendler,[‡] and Ioan Notingher*[,†]

[†]School of Physics and Astronomy and [‡]School of Pharmacy, University of Nottingham, Nottingham NG7 2RD, United Kingdom

[§]Faculty of Physics, Babes Bolyai University, Cluj-Napoca, Romania

Supporting Information

ABSTRACT: Polarized Raman microspectroscopy and atomic force microscopy were used to obtain quantitative information regarding the molecular structure of individual diphenylalanine (FF) nano- and microtubes. The frequencies of the Raman spectral bands corresponding to the amide I (1690 cm^{-1}) and amide III (1249 cm^{-1}) indicated that the FF-molecules interact by hydrogen bonding at the N−H and not at the C═O sites. The calculated mean orientation angles of the principal axes of the Raman tensors (PARTs) obtained from the polarized Raman spectral measurements were 41 ± 4° for the amide I and 59 ± 5° for amide III. On the basis of the orientation of the PART for the amide I mode, it was found that the C═O bond is oriented at an angle of 8 ± 4° to the tube axis. These values did not vary significantly with the diameter of the tubes (range 400−1700 nm) and were in agreement with the molecular structure proposed previously for larger crystalline specimens.

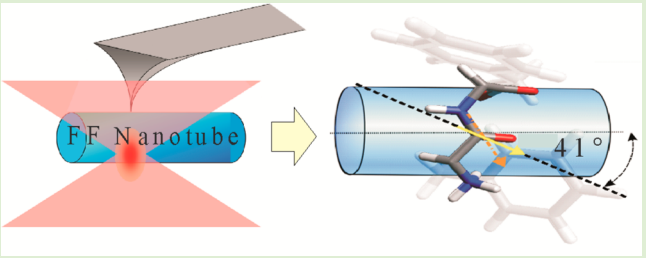

INTRODUCTION

Self-assembly of molecules is a powerful technique for the engineering of nanoscale materials. This so-called bottom-up approach exploits molecular recognition patterns based on a balance between thermodynamic and kinetic processes. Biological molecules, such as peptides, are ideal building blocks for designing nanostructures by self-assembly because of their specific molecular recognition patterns and the opportunities to manipulate them for specific functions. Here we consider the structures formed by one of the most versatile self-assembling peptides, diphenylalanine (L-Phe-L-Phe, FF). This dipeptide can be used as a building block for fabrication of biocompatible nanostructures with various forms (such as nanotubes and spherical constructs) with defined chemical and physical properties. On the basis of these unique features, such as mechanical rigidity,[1] thermal stability,[2] and biocompatibility, recent reports have proposed the use of FF-based nanostructures for biosensing, bioimaging, drug delivery, and 3D tissue culture scaffolds.[3] Whereas self-assembly is also responsible for many biological structures important for the normal functionality of healthy cells (lipid membranes and DNA), aberrant aggregation of proteins and peptides can lead to pathological conditions such as neurodegenerative diseases. The diphenylalanine peptide is itself the core recognition motif for self-assembly of the β-amyloid peptide associated with Alzheimer's disease.[4]

Although these FF-based nanostructures have been used extensively, experimental data regarding their structural organization and the molecular mechanisms involved in their formation from direct measurements on individual nano- or microtubes is still absent. Investigations of individual FF nanotubes have been carried out by various techniques, focused mainly on physical properties such as stiffness and strength[5] and thermal stability.[6] The molecular organization of self-assembled FF nanotubes was proposed based on a series of theoretical and X-ray diffraction (XRD) measurements carried out on needle-shaped crystals (not tubes) with dimensions 550 × 26 × 24 μm and FF powder.[7−11] On the basis of these experimental results, the individual FF nanotubes were proposed to consist of an aggregation of hollow tubular channels with water molecules positioned on the inside. Each individual FF channel is formed by stacking of ring-like structures of six molecules of zwitterionic FF ($+H_3N$-Phe-Phe-COO^-) where the adjacent molecules interact by head (NH_3^+)-to-tail (COO^-) hydrogen bonds and the side-chain aromatic rings form a 3-D stacking. However, one of the difficulties when extrapolating information obtained from measurements on ensembles or macroscopic samples is that the FF nanotubes usually show a broad distribution in the diameters, which may

Received: April 17, 2012
Revised: June 1, 2012
Published: June 4, 2012

dx.doi.org/10.1021/bm3005929 | Biomacromolecules 2012, 13, 2181−2187

result from different assembly pathways and hence, alternate molecular structures. Such diverse structural organization may be lost in the averaging related to X-ray diffraction analysis. Therefore, the proposed model based on X-ray diffraction data has not yet been scrutinized by any direct experimental observation on an individual nano- or microtube level.

Polarized Raman microspectroscopy can provide detailed information on molecular conformation together with orientation of the molecular bonds in a sample.[12−15] This technique has been used to study the structural organization in many types of materials, including inorganic nanotubes,[16,17] polymers,[18] and proteins.[19−22] The orientation of molecular bonds contributing to a vibrational mode of a molecule within a rigid matrix can be determined from polarized Raman spectroscopy measurements.[12] Details of the analytical method used in this study are included in the Supporting Information.

In this study, we have used polarized Raman spectroscopy measurements to investigate the molecular interactions and structure directly at a single FF nano- and microtube level. After the band assignment was completed by comparing the experimental spectra with the bands calculated by the density functional theory (DFT), simultaneous polarized Raman microspectroscopy and atomic force microscopy (AFM) measurements were used to determine the orientation of the amide bonds and the level of hydrogen bonding for FF nano- and microtubes with diameters in the range of 400−1700 nm.

EXPERIMENTAL SECTION

FF Nano- And Microtubes. All peptide solutions were prepared by initially solubilizing lyophilized L-diphenylalanine (FF) peptide (Genosphere, France) in 1,1,1,3,3,3-hexafluoro-2-propanol (HFIP) (Sigma Aldrich) to give a stock solution of 100 mg/mL. Stock solutions were further diluted to a working concentration of 2 mg/mL using ultrapure water (pH 7, resistivity 18.2 MΩ cm). Peptide solutions were vortexed mixed for 15 s to ensure complete dispersion and mixing of the sample in each stage of the preparation. A drop of the above solution was placed onto clean quartz coverslips and dried in a vacuum desiccator for ∼1 h at room temperature.

Raman Spectroscopy Measurements. The instrument used in this study consisted of an in-house polarized Raman microspectrometer based on an inverted optical microscope and integrated atomic force microscope, which was described in detail elsewhere.[23] For the polarized Raman spectroscopy measurements, a Glan-Thompson polarizer, serving as an analyzer, was placed in front of the spectrometer slit to allow the selection of a particular polarization direction for the Raman scattered light. A quarter-wave plate was introduced for scrambling the polarization of the collected light after the analyzer. The polarization directions of the excitation laser were selected by using a half-wave plate placed in the laser path. Correction factors of each polarization configuration were obtained from the polarized Raman measurements of carbon tetrachloride (CCl_4). A total of 12 FF tubes were investigated with 12 sets of polarized Raman spectra acquired from each tube. The set of polarized spectra consisted of four spectra (*ZZ*, *ZX*, *XZ*, *XX*) obtained with different polarization configurations (shown in the inset drawing in Figure 2). The first index denotes the laser polarization, and the second index represents the direction of the analyzer, while the excitation laser and the Raman backscattered radiation propagated in the *Y* direction. For each FF nanotube, polarized spectra were acquired from five positions at 3 μm step size. For all measurements, the nanotube axis was aligned along the *Z* direction. Each spectrum was acquired at 10 mW laser power with 10 s of acquisition time. To ensure that the laser did not induce damage to the nanotubes or changes in the Raman spectra, a singular value decomposition (SVD) analysis was carried out on 20 consecutive Raman spectra measured at single points of the nanotubes at 2 mW and 20 mW laser power and integration times of 50 and 10 s per spectrum. The SVD analysis indicated that the spectra can be described by a single significant singular value demonstrating that the consecutive Raman spectra were identical within the noise level (Supporting Information, Figure S2).

Theoretical Calculation. The geometry optimization and the Raman spectrum were computed using the Gaussian 09 software package[24] by using DFT with B3LYP hybrid exchange-correlation functional.[25,26] For the expansion of the orbitals, the 6-31++G(d, p) splitting valence basis set with diffuse and polarization functions was used. The input molecule was taken from the crystallographic data reported by Görbitz.[7] Given the unusual conformation of the FF molecule, dihedral angles constraints were imposed to maintain the arrangement of the molecule. A geometry optimization calculus was performed in water solvent using the conductor-like polarizable continuum model (CPCM) method.[27] After geometrical optimization, a frequency calculation was performed to predict the Raman spectrum of the molecule. Prior to comparing the calculated vibrational frequencies with the experimental counterparts, the former were scaled by appropriate scaling factors.[28] The observed experimental bands were assigned by visual inspection of the vibrations using the animated feature of the Gauss View 4.1 program, considering both the frequency sequence and intensity pattern and by comparisons with the vibrational spectra of similar compounds.

RESULTS AND DISCUSSION

Band Assignment and Hydrogen Bonding. Figure 1 presents the unpolarized Raman spectrum of a typical FF

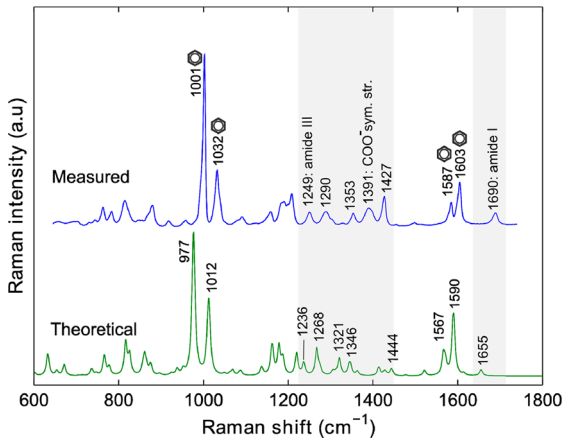

Figure 1. Typical measured Raman spectrum of a FF nanotube and the theoretical spectrum calculated by Gaussian09.

nanotube and the theoretical calculated spectrum for the FF molecule in water. The very close agreement between the shapes (band positions and relative intensities) of the two spectra supports the proposed conformation of the FF molecules in which the phenyl side chains are located on the same side of the plane defined by the peptide bond.[7] However, differences in the band frequencies of ∼10−20 cm^{-1} were noticed, which can be attributed to the different conditions of the FF molecules within the nanotubes compared with those considered within the solvation model of the theoretical calculation. Considering these differences, only the shape and intensity pattern of the Raman bands in the theoretical spectrum were used for the assignment of the experimentally observed bands.

This assignment was confirmed by the theoretical spectrum, which showed a band at 1655 cm^{-1} dominated by the carbonyl C═O stretching with a lower contribution of C−N stretching. It is interesting to note that the 1690 cm^{-1} band appears at a rather high frequency compared with other dipeptides.[29] This

high-frequency amide I band indicates that the dipeptides do not interact by hydrogen bonding at the carbonyl group. For the isolated C═O bond, the amide I band is found around 1700 cm^{-1}; hydrogen bonding significantly affects the charge distribution and bond length, which results in a frequency downshift of up to 33 cm^{-1}.[30] It has been showed that hydrogen bonding at the N−H side can also affect the length of the C═O and thus shift the frequency of the amide I band. However, the shift caused by hydrogen bonding at the N−H is significantly lower than when the hydrogen bonding is at the C═O sites.[30] The decrease in the electron density at the peptide hydrogen due to hydrogen bonding at N−H increases the charge density at the other peptide atoms. This redistribution of the charge density can lead to an increase in the C═O bond of ∼37% compared with when the hydrogen bonding is at C═O site and thus a downshift the amide I band of only ∼10 cm^{-1}.[30] Therefore, the 1690 cm^{-1} frequency of the amide I band is consistent with hydrogen bonding at the N−H and no hydrogen bonding at C═O, in agreement with the proposed structure of the FF nanotubes.[7,10] Figure 2 presents the AFM images and the polarized Raman spectra corresponding to typical FF nanotube (400 nm diameter) and microtube (1443 nm diameter) (tube heights as measured by AFM). For

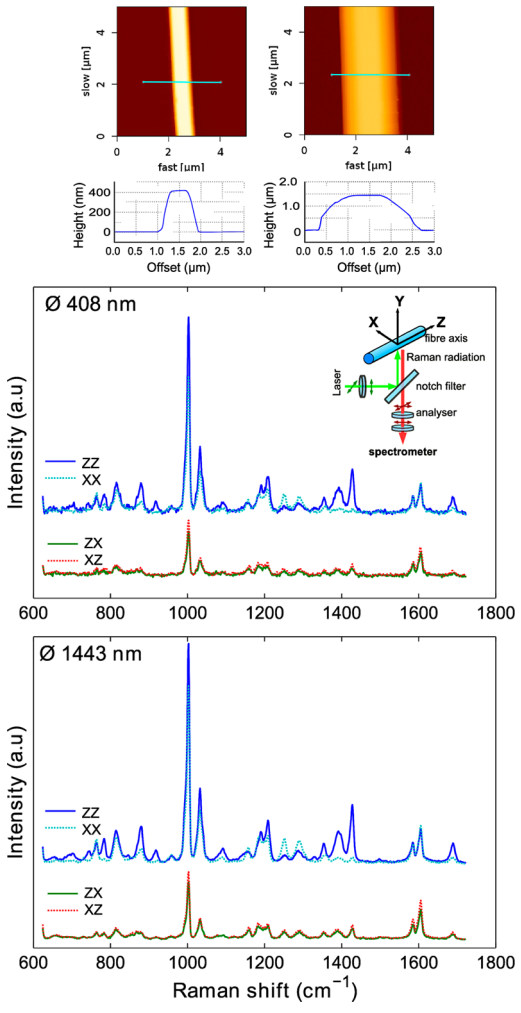

Figure 2. AFM images of individual FF nano- and microtube and their corresponding polarized Raman spectra. The polarization configurations are shown in the inset drawing.

both tubes, the amide I bands exhibit higher intensity in the *ZZ* conformation compared with the *XX* configuration, suggesting that the principal axis of the Raman tensor (PART) of this vibration aligns preferentially along the tube axis.

In peptides, polypeptides, and proteins, the vibrational bands arising in the 1200−1300 cm^{-1} region are typically attributed to amide III vibrations. These bands correspond to the combination of C−N stretchings, N−H in-plane bendings, C_α-C stretchings, and C═O in-plane bendings.[31] The Raman spectra of FF tubes show two main Raman bands in this spectral region (Figures 1 and 2) at 1249 and 1290 cm^{-1}. To identify which of the two bands corresponds to the amide III vibrations, we based the assignment of these bands on the calculated spectrum of FF in water. A more detailed view of the experimental and computed spectra in the 1200−1350 cm^{-1} region is presented in Figure 3 along with the schematic

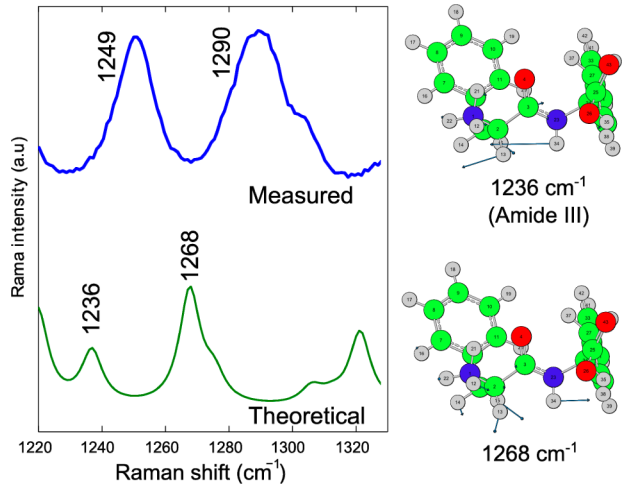

Figure 3. Comparison between the measured and theoretical Raman spectra in the 1220−1330 cm^{-1} range. The molecular vibrations corresponding to the theoretical calculation are displayed on the right.

molecular vibrations contributing to the bands in the computed spectrum. The lower frequency band at 1236 cm^{-1} has strong contributions from the amide III mode as well as C_α-H in-plane bending. The higher mode at 1268 cm^{-1} corresponds to a mixed vibration consisting of C_β-H bending, C_α-H out-of-plane bending, N−H in-plane bending, and C_α-C_β stretching. On the basis of this comparison, only the 1249 cm^{-1} band in the experimental spectrum was assigned to the amide III vibrational mode. It has been pointed out that the frequency of the amide III band depends on the properties of the backbone and peptide bond and conformation of peptides as well as hydrogen bonding at the N−H and C═O sites. According to Asher et al.,[32,33] the position of the amide III band can be correlated to the Ramachandran dihedral Ψ angle, whereas the Ramachandran Φ angle contributes much less to the frequency shift. The observed low frequency of the amide III in the Raman spectrum of the FF tubes (1249 cm^{-1}) supports the strong coupling between the N−H and C_α-H in-plane bending motions, which is also indicated by the theoretical spectrum. This strong coupling is consistent with the Ramachandran dihedral Ψ angle of 157 observed in the X-ray data. For such values of Ψ, the cis conformation of N−H and the C_α-H bonds leads to an overlap of the van der Waals radii of the two H atoms; therefore, the strong coupling between N−H and the C_α-H in-plane bending can downshift the amide III frequency

dx.doi.org/10.1021/bm3005929 | *Biomacromolecules* 2012, 13, 2181−2187

by up to 100 cm^{-1}.[33] However, hydrogen bonding at either N−H or C═O sites can also lead to upshifts in the vibration frequency of the amide III band. Compared with the amide I, the amide III is equally affected by hydrogen bonding at N−H and C═O, with reported upshifts of 22 and ∼23 cm^{-1}, respectively.[30]

Because the high frequency of the amide I indicated no hydrogen bonding at the C═O, the 1249 cm^{-1} frequency for the amide III can be attributed to hydrogen bonding at the N−H suggested by the theoretical structure of the FF nanotubes.[7,10] The polarization dependence of the amide III band is noticeable in Figure 2 as the intensity in the *XX* configuration is higher than in the *ZZ* configuration. Therefore, it can be implied that the PART of the amide III vibration is likely oriented perpendicular to the axis of the nanotubes.

In the case of peptides, such characteristics have been intensively studied by Tsuboi et al.[34−36] and Pajcini et al.,[37] and the localized polarizability tensors for the amide vibrations have been obtained. However, it has been highlighted that the tensors of various vibrational modes cannot always be transferred between different peptide and protein structures.[34−36] Previous work has showed that the tensor for the amide I vibration maintains its shape regardless of its molecular environment,[34−36] but the transferability of the amide III tensor has not yet been demonstrated experimentally. However, considering the highly localized nature of this normal mode of vibration, our quantitative analysis was applied to both amide I and amide III vibrations, and it was based on the tensors reported by Pajcini et al.[37] These tensors were converted to make their largest element (α_3 normalized to unity) of PART parallel to the *z* axis of the molecular frame, which correlates to the laboratory *Z* axis (tube axis) through the Euler angle θ (Supporting Information Figure S1). The elements of these tensors for the amide I (1690 cm^{-1} and the amide III (1249 cm^{-1}) are presented in Table 1 in the form of ratios $r_1 = \alpha_1/\alpha_3$ and $r_2 = \alpha_2/\alpha_3$.

Table 1. Raman Polarizability Tensors Used in the Determination of Molecular Orientation for the Selected Vibrations Observed in the Raman Spectra of Self-Assembled FF Tubes[a]

band (cm^{-1})	assignment	r_1	r_2
1249	amide III	−0.085	0.356
1690	amide I	−0.016	0.274

[a]All tensors were adapted from Pajacini et al.[37]

The polarized Raman spectra in Figure 2 show that the spectra corresponding to the *ZX* and *XZ* configurations overlap almost completely, confirming that the conditions for using the uniaxial model are satisfied. In addition, no significant differences can be observed between the polarized Raman spectra corresponding to nano- and microtubes with different diameters. Figure 4 presents the calculated values of the ratios R_X and R_Z corresponding to the 1249 and 1690 cm^{-1} Raman bands for FF tubes with diameters ranging from 400 to 1700 nm. The markers present the averaged R_X and R_Z ratios of three repeated measurements at the same positions on a tube. For the amide I band, the mean values of R_X and R_Z for the nanotubes (diameter 400−700 nm) were 1.0 ± 0.2 and 0.44 ± 0.08, whereas for the microtubes (diameter 1000−1700 nm) the values were 1.0 ± 0.1 and 0.33 ± 0.03. Similarly close results were observed for the amide III, in which case the R_X and R_Z

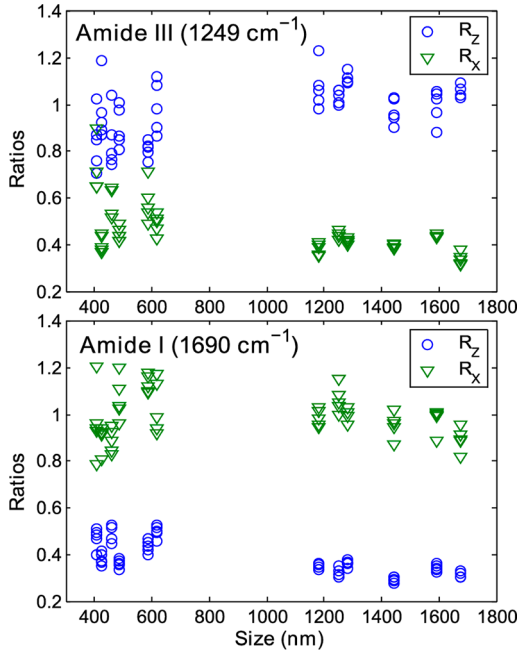

Figure 4. R_z and R_x intensity ratios for the amide III and the amide I Raman bands.

were 0.5 ± 0.1 and 0.9 ± 0.2 for the smaller nanotubes and 0.40 ± 0.05 and 1.0 ± 0.1 for the larger nanotubes. These results indicate that no significant differences were observed between the R_X and R_Z values between FF nanotubes with different diameters.

When using Raman microspectroscopy with high numerical aperture (NA) objectives in backscattering geometry, the accurate calculation of the orientation parameters requires the correction parameters *A* and *B* in eqs 2 and 3 of the the Supporting Information. Following Turrell[38] and Brémard,[39] for a microscope objective of NA = 1.2 and a typical refractive index of 1.4 for proteins, the correction parameters were *A* = 5.018 and *B* = 1.528. (See the Supporting Information.) Figure 5 presents the calculated orientation parameters $<P_2>$ and $<P_4>$ corresponding to the amide I and amide III Raman bands for FF nanotubes. Similar values (within the experimental uncertainties) were also obtained when using the Raman tensor reported by Tsuboi et al.[36] and when the refractive index of the FF tubes was varied in the range 1.2 to 1.6. As expected from the variability of the computed ratios R_x and R_z, the orientation parameters for the group of larger diameters show a significantly lower variability compared to the group of smaller diameters.

The variability of the ratios is mostly attributed to the inferior signal-to-noise ratio of the Raman spectra of the nanotubes, which consequently increased the error in calculation of the Raman bands. However, it is apparent that the mean values of the orientation parameters are very similar for all tubes regardless of diameters. The parameter $<P_2>$ in theory varies between −0.5 and 1, and these extreme values correspond to perpendicular and parallel orientations. The negative values of $<P_2>$ corresponding to the 1249 cm^{-1} band (amide III) for all FF nanotubes indicate that the PART is preferentially oriented perpendicular to the axis of the nanotubes. In contrast, the 1690 cm^{-1} Raman bands are characterized by positive values of $<P_2>$, suggesting that their corresponding PARTs are aligned predominantly along the nanotube axis.

dx.doi.org/10.1021/bm3005929 | *Biomacromolecules* 2012, 13, 2181−2187

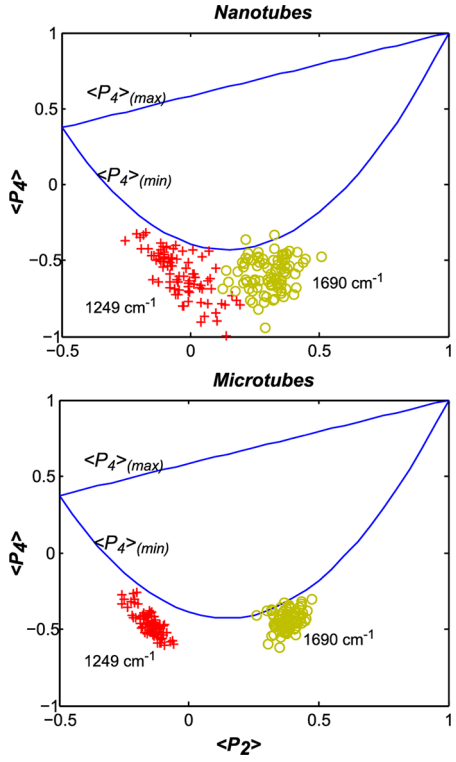

Figure 5. Scatter plots for the orientation parameters $\langle P_2 \rangle$ and $\langle P_4 \rangle$ corresponding to the amide I and amide III vibration modes of the FF nanotubes (diameters 400−700 nm) and microtubes (1000−1700 nm).

It has been shown that for a given $\langle P_2 \rangle$, only certain values of $\langle P_4 \rangle$ are possible given by the Schwarz's inequalities.[40] As can be seen in Figure 5, the plots $\langle P_2 \rangle$ versus $\langle P_4 \rangle$ of the 1249 and 1690 cm^{-1} Raman bands exhibit the same trend of scattering around the line $\langle P_4 \rangle = \langle P_4 \rangle_{min}$. Values falling outside the possible $\langle P_4 \rangle$ region are presumably due to the variability in measurements and uncertainty of the parameters used in the calculations (A, B, and the shape of localized Raman polarizability tensors). In the case of $\langle P_4 \rangle = \langle P_4 \rangle_{min}$, the orientation distribution function represents a delta function with a single peak at an angle given by[41]

$$\theta_0 = \arccos\left(\frac{2}{3}\langle P_2 \rangle + \frac{1}{3}\right)^{1/2}$$

Using the above equation, the orientation angle for the amide I and amide III modes can be calculated as shown in Table 2.

The results from Table 2 lead to the conclusion that the FF molecules that self-assemble to form tubes with diameters in the 400−1700 nm have similar orientations for both the amide I and amide III vibrational modes. The PART of the 1249 cm^{-1} band (amide III) creates the largest tilting angle (59 ± 5°), whereas the PART of the 1690 cm^{-1} band makes 41 ± 4° with the tube axis. As the PART corresponding to the amide I is oriented at 33° from the carbonyl C═O bond,[37] the C═O bonds are predominantly oriented at 8 ± 4° to the tube axis (Figure 6). This value is in good agreement with the predicted angle in the proposed structure of the FF nanotubes.[7,10]

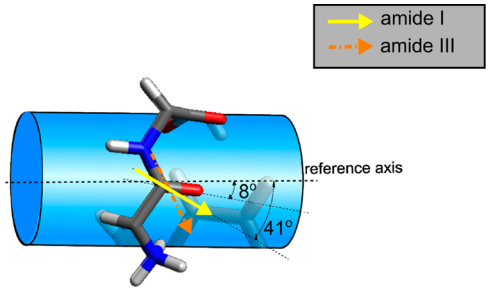

Figure 6. Schematic description of the FF tubes. The C═O bonds are not involved in H bonding and are predominantly oriented at 8 ± 4° relative to the tube axis. The amide N−H interacts by H bonding with the carboxylate group of the adjacent helix providing stability to the tubular structure.

The orientation of the carbonyl C═O can also be determined from the amide III vibration. The calculated PART makes an angle of 59 ± 5° to reference axis, whereas the PART is oriented 59° from the C═O bond (26° with the PART of the amide I).[37] This suggests that the carbonyl C═O should be oriented in the direction of 0 ± 5° to the nanotube axis. Although this value is close to the value obtained from the analysis of amide I, the difference can be attributed to the significant contribution of the C_α-H in-plane bending to the 1249 cm^{-1} band as well as to the transferability of the tensor for the amide III mode.

CONCLUSIONS

Raman microspectroscopy and AFM were used to investigate the molecular interactions and orientation of FF molecules after self-assembling into nano- and microtubes with diameters in the 400−1700 nm range. The integration of the AFM and Raman microscope allowed direct measurements on individual FF tubes for which the diameter was accurately determined. Calculations by DFT allowed the assignment of the 1249 cm^{-1} to the amide III vibration and indicated a strong coupling between C_α-H and N−H bending vibrations. Information regarding hydrogen bonding at the N−H and C═O sites of the peptide bond was obtained from the frequencies of the amide I and amide III bands. The high position of the amide I (1690 cm^{-1}) indicated that only the N−H was involved in hydrogen bonding. The same conclusion was reached from the analysis of the amide III band (1249 cm^{-1}). These additional H bonding interactions between the amide N−H and the carboxylate groups of adjacent helices may contribute to the rigidity of the tubular structures formed by FF molecules.

The orientation of the PARTs corresponding to the dipeptide backbone, amide I and amide III, were determined

Table 2. Averaged Values for All FF Tubes of the Intensity Ratios R_Z, R_X, Orientation Parameters $\langle P_2 \rangle$ and $\langle P_4 \rangle$ and the Angle (With Respect to the Nanotube Axis) of the PART Raman Polarizability Tensors Corresponding to the Amide III and Amide I Modes

band (cm^{-1})	R_Z	R_X	$\langle P_2 \rangle$	$\langle P_4 \rangle$	θ (deg)
1249	1.0 ± 0.2	0.5 ± 0.1	−0.1 ± 0.1	−0.6 ± 0.2	59 ± 5
1690	0.38 ± 0.08	1.0 ± 0.2	0.3 ± 0.1	−0.5 ± 0.1	41 ± 4

dx.doi.org/10.1021/bm3005929 | Biomacromolecules 2012, 13, 2181−2187

based on the calculation of intensity ratios corresponding to these bands in the polarized Raman spectra. The mean orientation angles of the tensors were 41 ± 4 and 59 ± 5° for the amide I and amide III respectively, which correspond to orientation angles of the carbonyl C═O bond of 8 ± 4 and 0 ± 5°. The small difference in the orientation angle of the C═O bond may be due to the contribution of the C_α-H vibrations to the 1249 cm^{-1} band and the assumption that the tensor of the amide III does not depend on the environment of the peptide bond. These results are in good agreement with the molecular structure proposed previously based on X-ray data obtained for macroscopic crystalline specimens. Because no significant differences were found between FF nano- and microtubes with different diameters, these results may suggest that the actual molecular configurations of the FF tubes are similar regardless of the diameters and shapes of the tubes.

■ ASSOCIATED CONTENT

Ⓢ Supporting Information

Theoretical model for polarized Raman microspectroscopy, representation of the *XYZ* laboratory coordinate frame and the *xyz* system representing the coordinate frame of the molecule, and evidence that the laser exposure did not induce changes in the Raman spectra of the FF nanotubes.

This material is available free of charge via the Internet at http://pubs.acs.org.

■ AUTHOR INFORMATION

Corresponding Author

*E-mail: ioan.notingher@nottingham.ac.uk.

Notes

The authors declare no competing financial interest.

■ ACKNOWLEDGMENTS

This study was supported by grant awards from the University of Nottingham.

■ REFERENCES

(1) Kol, N.; Adler-Abramovich, L.; Barlam, D.; R. Shneck, Z.; Gazit, E.; Rousso, I. Self-Assembled Peptide Nanotubes Are Uniquely Rigid Bioinspired Supramolecular Structures. *Nano Lett.* **2005**, *5*, 1343−1346.

(2) Adler-Abramovich, L.; Reches, M. V.; Sedman, L.; Allen, S.; Tendler, S. J. B.; Gazit, E. Thermal and Chemical Stability of Diphenylalanine Peptide Nanotubes: Implications for Nanotechnologycal Applications. *Langmuir* **2006**, *22*, 1313−1320.

(3) Yan, X.; Zhu, P.; Li, J. Self-assembly and application of diphenylalanine-based nanostructures. *Chem. Soc. Rev.* **2010**, *39*, 1877−1890.

(4) Reches, M.; Gazit, E. Casting metal nanowires within discrete self-assembled peptide nanotubes. *Science* **2003**, *300*, 625−627.

(5) Niu, L.; Chen, X.; Allen, S.; Tendler, S. J. B. Using the Bending Beam Model to Estimate the Elasticity of Diphenylalanine Nanotubes. *Langmuir* **2007**, *23*, 7443−7446.

(6) Sedman, V. L.; Allen, S.; Chen, X.; Roberts, C. J.; Tendler, S. J. B. Thermomechanical Manipulation of Aromatic Peptide Nanotubes. *Langmuir* **2009**, *25*, 7256−7259.

(7) Görbitz, C. H. Nanotubes formation by Hydrophobic Dipeptides. *Chem.—Eur. J.* **2001**, *7*, 5153−5159.

(8) Görbitz, C. H. An exceptionally stable peptide nanotube system with flexible pores. *Acta Cryst. Sect. B* **2002**, *58*, 849−854.

(9) Görbitz, C. H. Nanotubes from hydrophpbic dipeptides: pore size regulation through side chain substitution. *New J. Chem.* **2003**, *27*, 1789−1893.

(10) Görbitz, C. H. The structure of nanotubes formed by diphenylalanine, the core recognition motif of Alzheimer's b-amyloid polypeptide. *Chem. Commun.* **2006**, 2332−2334.

(11) Tamamis, P.; Adler-Abramovich, L.; Gazit, E.; Archontis, G. Insights into the Self-Assembly of Phenylalanine Oligopeptides by Replica Exchange MD Simulations with the GBSW Implicit-Solvent Model. *CBSB08 Proceedings* **2008**, *40*, 393−396.

(12) Bower, D. I. Investigation of Molecular Orientation Distributions by Polarized Raman Scattering and Polarized Fluorescence. *J. Polym. Sci.* **1972**, *10*, 2135−2153.

(13) Sourisseau, C. Polarization Measurements in Macro- and Micro-Raman Spectroscopies: Molecular Orientations in Thin Films and Azo-Dye Containing Polymer system. *Chem. Rev.* **2004**, *104*, 3851−3891.

(14) Ikeda, R.; Chase, B.; Everall, N. Basics of Orientation Measurements in Infrared and Raman Spectroscopy. *Hanbook of Vibrational Spectroscopy* **2002**, *1*, 716−730.

(15) Lagugné-Labarthet, F. Polarized measurements in Raman microscopy. *Annu. Rep. Prog. Chem., Sect. C* **2007**, *103*, 326−350.

(16) Duesberg, G. S.; Loa, I.; Burghard, M.; Syassen, K.; Roth, S. Polarized Raman spectroscopy on Isolated Single-Wall Carbon Nanotubes. *Phys. Rev. Lett.* **2000**, *85*, 5436−5439.

(17) Chien, C.; Wu, M.; Chen, C.; Yang, H.; Wu, J.; Su, W.; Lin, C.; Chen, Y. Polarization-dependent confocal Raman microscopy of an individual ZnO nanorod. *Appl. Phys. Lett.* **2008**, *92*, 223102.

(18) Song, K.; Rabolt, J. F. Polarized Raman measurements of Uniaxially Oriented Poly (ε-caprolactam). *Macromolecules* **2001**, *34*, 1650−1654.

(19) Rousseau, M.; Lefèvre, T.; Beaulieu, L.; Asakura, T.; Pézolet, M. Study of Protein Conformation and Orientation in Silkworm and Spider Silk Fibers Using Raman Microspectroscopy. *Biomacromolecules* **2004**, *5*, 2247−2257.

(20) Rousseau, M.; Beaulieu, L.; Lefèvre, T.; Paradis, J.; Asakura, T.; Pézolet, M. Characterization by Raman Microspectroscopy of the Strain-Induced Conformational Transition in Fibroin Fibers from the Silkworm *Samia Cynthia ricini*. *Biomacromolecules* **2006**, *7*, 2512−2521.

(21) Falgayrac, G.; Facq, S.; Leroy, G.; Cortet, B.; Penel, G. New Method for Raman Investigation of the Orientation of Collagen Figrils and Crystallites in the Haversian System of Bone. *Appl. Spectrosc.* **2010**, *64*, 775−780.

(22) Janko, M.; Davydovskaya, P.; Bauer, M.; Zink, A.; Stark, W. R. Anisotropic Raman scattering in collagen bundles. *Opt. Lett.* **2010**, *35*, 2765−2767.

(23) Sweetenham, C. S.; Larraona-Puy, M.; Notingher, I. Simultaneous SERS and AFM for label-free physicochemical analysis of lipid bilayers. *Appl. Spectrosc.* **2011**, *65*, 1387−1392.

(24) Frisch, M. J.; Trucks, G. W.; Schlegel, H. B.; Scuseria, G. E.; Robb, M. A.; Cheeseman, J. R.; Scalmani, G.; Barone, V.; Mennucci, B.; Petersson, G. A.; et al. Gaussian 09, Revision A.1, Gaussian, Inc., Wallingford CT, 2009.

(25) Becke, A. D. Density-functional thermochemistry. III. The role of exact exchange. *J. Chem. Phys.* **1993**, *98*, 5648−5652.

(26) Lee, C.; Yang, W.; Parr, R. G. Development of the Colle-Salvetti conelation energy formula into a functional of the electron density. *Phys. Rev. B* **1988**, *37*, 785−789.

(27) Cossi, M.; Rega, N.; Scalmani, G.; Barone, V. Energies, Structures, and Electronic Properties of Molecules in Solution with the C-PCM Solvation Model. *J. Comput. Chem.* **2003**, *24*, 669−681.

(28) Merrick, J. P.; Moran, D.; Radom, L. An Evaluation of Harmonic Vibrational Frequency Scale Factors. *J. Phys. Chem. A* **2007**, *111*, 11683−11700.

(29) Podstawka, E.; Ozaki, Y.; M. Proniewicz, L. Part I: Surface-Enhanced Raman Spectroscopy Investigation of Amino Acids and Their Homodipeptides Adsorbed on Colloidal Silver. *Appl. Spectrosc.* **2004**, *58*, 570−580.

(30) Myshakina, N. S.; Ahmed, Z.; Asher, S. A. Dependence of Amide Vibrations on Hydrogen Bonding. *J. Phys. Chem. B* **2008**, *112*, 11873−11877.

(31) Krimm, S.; Bandekar, J. Vibrational Spectroscopy and Conformation of Peptides, Polypeptides, and Proteins. *Adv. Protein Chem.* **1986**, *38*, 181−364.
(32) Asher, S. A.; Ianoul, A.; Mix, G.; Boyden, M. N.; Karnop, A.; Diem, M.; Schweitzer-Stenner, R. Dihedral ψ Angle Dependence of the Amide III Vibration: A Uniquely Sensitive UV Resonance Raman Secondary Structure Probe. *J. Am. Chem. Soc.* **2001**, *123*, 11775−11781.
(33) Mikhonin, A. V.; Bykov, S. V.; Myshakina, N. S.; Asher, A. S. Peptide Secondary Structure Folding Reaction Coordinate: Correlation between UV Raman Amide III Frequency, ψ Ramachandran Angle, and Hydrogen Bonding. *J. Phys. Chem. B* **2006**, *110*, 1928−1943.
(34) Tsuboi, M.; Ezaki, Y.; Aida, M.; Suzuki, M.; Yimit, A.; Ushizawa, K.; Ueda, T. Raman Scattering Tensors of Tyrosine. *Biospectroscopy* **1998**, *4*, 61−71.
(35) Tsuboi, M.; Ikeda, T.; Ueda, T. Raman Microscopy of Small Uniaxial Crystal: Tetragonal Aspartame. *J. Raman Spectrosc.* **1991**, *12*, 619−629.
(36) Tsuboi, M.; Ueda, T.; Ushizawa, K. Localized Raman tensors in some biopolymers. *J. Mol. Struct.* **1995**, *352/353*, 509−517.
(37) Pajcini, V.; Chen, X. G.; Bormett, R. W.; Geib, S. J.; Li, P.; Asher, S. A.; Lidiak, E. G. Glycylglycine $\pi \rightarrow \pi^*$ and Charge Transfer Transition Moment Orientations: Near-Resonance Raman Single-Crystal Measurements. *J. Am. Chem. Soc.* **1996**, *118*, 9716−9726.
(38) Turrell, G. Analysis of Polarization Measurements in Raman Microspectroscopy. *J. Raman Spectrosc.* **1984**, *15*, 103−108.
(39) Brémard, C.; Laureyns, J.; Merlin, J.; Turrell, G. Polarization Measurements in Raman Microspectroscopy. *J. Raman Spectrosc.* **1987**, *18*, 305−313.
(40) Nomura, S.; Kawai, H.; Kimura, I.; Kagiyama, M. General description of orientation factors in terms of expansion of orientation distribution function in a series of spherical harmonics. *J. Polymer Sci. A2* **1970**, *8*, 383−400.
(41) Potel, H.; Herreman, W.; van der Meer, B. W.; Ameloot, M. On the significance of the fourth-rank orientational order parameter of fluorophores in membrances. *Chem. Phys.* **1986**, *102*, 37−34.